



HAL
open science

Hydro-mechanical modeling of internal erosion in dike

Jie Yang, Farid Laouafa, Zhen-Yu Yin, Pierre-Yves Hicher

► **To cite this version:**

Jie Yang, Farid Laouafa, Zhen-Yu Yin, Pierre-Yves Hicher. Hydro-mechanical modeling of internal erosion in dike. 53. US Rock Mechanics / Geomechanics Symposium, Jun 2019, New York, United States. ineris-03237762

HAL Id: ineris-03237762

<https://ineris.hal.science/ineris-03237762>

Submitted on 26 May 2021

HAL is a multi-disciplinary open access archive for the deposit and dissemination of scientific research documents, whether they are published or not. The documents may come from teaching and research institutions in France or abroad, or from public or private research centers.

L'archive ouverte pluridisciplinaire **HAL**, est destinée au dépôt et à la diffusion de documents scientifiques de niveau recherche, publiés ou non, émanant des établissements d'enseignement et de recherche français ou étrangers, des laboratoires publics ou privés.

Hydro-mechanical modeling of internal erosion in dike

Jie YANG

INERIS, Verneuil en Halatte, France; Research Institute of Civil Engineering and Mechanics (GeM), UMR CNRS 6183, Ecole Centrale de Nantes, France

Farid LAOUAFA*

INERIS, Verneuil en Halatte, France, E-mail: farid.laouafa@ineris.fr

Zhen-Yu YIN

Department of Civil and Environmental Engineering, The Hong Kong Polytechnic University, Hung Hom, Kowloon, Hong Kong, China

Pierre-Yves HICHER

Research Institute of Civil Engineering and Mechanics (GeM), UMR CNRS 6183, Ecole Centrale de Nantes, France

Copyright 2019 ARMA, American Rock Mechanics Association

This paper was prepared for presentation at the 53rd US Rock Mechanics/Geomechanics Symposium held in New York, NY, USA, 23–26 June 2019. This paper was selected for presentation at the symposium by an ARMA Technical Program Committee based on a technical and critical review of the paper by a minimum of two technical reviewers. The material, as presented, does not necessarily reflect any position of ARMA, its officers, or members. Electronic reproduction, distribution, or storage of any part of this paper for commercial purposes without the written consent of ARMA is prohibited. Permission to reproduce in print is restricted to an abstract of not more than 200 words; illustrations may not be copied. The abstract must contain conspicuous acknowledgement of where and by whom the paper was presented.

ABSTRACT: Instability in geotechnical structures such as dikes or earth dams may be induced by internal erosion. In this phenomenon, finer soil particles are plucked off from the solid matrix by seepage flow and transported through the pore domain over time. Due to the loss of a part of the solid phase, the mechanical properties of the soil are progressively degraded, and, with time, earthen structures are under considerable risk of failure. Research on this topic is still fairly new and much more needs to be understood. In this study, a hydro-mechanical model based on porous continuous medium theory has been proposed to assess how internal erosion impacts the safety of earthen structures. An elasto-plastic constitutive model for sand-silt mixtures has been developed to describe the effect of the evolution of both porosity and fines content induced by internal erosion upon the behavior of the soil skeleton. The model is developed within finite element method framework. It is applied to a dike subjected to internal erosion induced by the presence of a karstic cavity beneath the alluvium layer.

1. INTRODUCTION

Internal erosion occurs when fine particles are plucked off by hydraulic forces and transported through the coarse matrix. The known causes are either a concentration of leak erosion, backward erosion, soil contact erosion, or suffusion (Bonelli and Marot 2008; Fell et al. 2003; Wan and Fell 2004). This paper focuses on suffusion, which corresponds to the detachment and migration of fine particles within the voids of coarse particles by seepage flow. The induced modification of the soil microstructure may lead to deformations at the macroscopic scale and, consequently, influence significantly the mechanical behavior of the soil. Many damages and failures of embankment dams can be associated with internal erosion (Fell et al. 2003; Xu and Zhang 2009; Zhang and Chen 2006; Zhang et al. 2009; Rönnqvist et al. 2014). Foster et al. (2000) showed that internal erosion led to nearly 46% of the damages of 128 embankment dams. Besides, sinkholes and cavities triggered by internal erosion are frequently observed within dams and dikes (Muir Wood 2007; Sterpi 2003). Internal erosion can also trigger slope

failures and generate significant landslides (Crosta and Prisco 1999; Hu et al. 2018).

Over the last decades, this phenomenon has been tested in the laboratory (Bendahmane et al. 2008; Bendahmane et al. 2006; Chang and Zhang 2011; Marot et al. 2016; Moffat et al. 2011; Reddi et al. 2000; Skempton and Brogan 1994; Sterpi 2003). The focus has been on the potential for internal erosion, its initiation and development under multi-stage seepage flows and complex stress states, as well as on the stress-strain behavior of eroded soils. More recently, internal erosion has been modeled by several numerical methods in order to enhance the design of hydraulic works. All these studies have adopted either a discrete approach (Lominé et al. 2013; Reboul 2008; Sari et al. 2011; Scholtès et al. 2010; Sibille et al. 2015; Zhao and Shan 2013) or a continuous approach (Bear and Bachmat 2012; Cividini and Gioda 2004; Fujisawa et al. 2010; Schaufler et al. 2013; Stavropoulou et al. 1998; Vardoulakis et al. 1996; Wong et al. 2013).

Since the continuous approach permits work to be done at the scale of an entire engineering structure, it is certainly

preferable to operate within this framework and to improve the mechanical response of the soil by monitoring the porosity and the evolution of the fines content throughout the process of internal erosion. First, a four-constituent model has been developed to describe the detachment and transport of fines content induced by internal erosion. It was implemented into a finite element and validated by reproducing a wellbore erosion simulation. Secondly, the solid skeleton behavior has been simulated by a novel elasto-plastic sand-silt mixture model which accounts for the effect of porosity and fines content on the degraded mechanical properties of the soil to analyze the influence of internal erosion induced by the collapse of a karstic cavity beneath the alluvium layer of a dike.

2. MODEL FORMULATIONS

2.1. Mass balance and particle transport

The mass balance equations are based on the porous media theory (de Boer 2000; Schaufler et al. 2013; Yang et al. 2017). The saturated porous medium is modeled as a system of 4 constituents: the solid skeleton (*ss*), the erodible fines (*se*), the fluidized particles (*fp*) and the pure fluid (*ff*), as shown in Fig. 1. The fines can either behave as a fluid-like (described as fluidized particles) or a solid-like (described as erodible fines) material. Thus, a liquid-solid phase transition process is taken into account in the present model by a mass production term in the corresponding mass balances for erodible fines and fluidized particles.

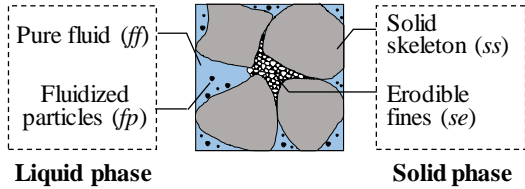


Fig. 1. Microstructure of fluid saturated granular soils

In a given Representative Elementary Volume (dV) consisting of the four constituents, the volume fraction n^x of a single constituent x is expressed as:

$$n^x = dV^x / dV \quad (1)$$

with dV^x denoting the volume of the corresponding constituent.

At a material point level, the volume balance for the x phase is reduced from the mass balance, neglecting the hydro-mechanical dispersion tensor (Schaufler et al. 2013):

$$\partial_t (n^x) + \text{div}(n^x \mathbf{v}^x) = n^{\text{ex},x} \quad (2)$$

where $n^{\text{ex},x}$ is the volume exchange term, \mathbf{v}^x is the velocity.

Moreover, it is assumed that fluid and fluidized particles have at any time the same velocity. The solid skeleton is assumed to be deformable but non-erodible. The porosity field ϕ , the amount of erodible fines f_c , the concentration of the fluidized particles c are defined as follows:

$$\phi = n^{\text{ff}} + n^{\text{fp}}, f_c = n^{\text{se}} / (1 - \phi) \text{ and } c = n^{\text{fp}} / \phi \quad (3)$$

The transformation of the state of fines from part of the solid skeleton to fluidized particles leads to:

$$n^{\text{ex},a} = -n^{\text{ex},se} = \hat{n}, n^{\text{ex},ss} = 0 \text{ and } n^{\text{ex},ff} = 0 \quad (4)$$

The mass balance equations are then given by the following expressions:

$$-\partial_t \phi + \text{div}(\mathbf{v}_s) - \text{div}(\phi \mathbf{v}_s) = -\hat{n} \quad (5)$$

$$\partial_t (f_c) - \partial_t (f_c \phi) + \text{div}(f_c \mathbf{v}_s) - \text{div}(f_c \phi \mathbf{v}_s) = -\hat{n} \quad (6)$$

$$\partial_t (c\phi) + \text{div}(c\mathbf{q}_w) + \partial_t (c\phi \mathbf{v}_s) = \hat{n} \quad (7)$$

$$\text{div}(\mathbf{q}_w) + \text{div}(\mathbf{v}_s) = 0 \quad (8)$$

Where \mathbf{q}_w denotes the total discharge of liquid, $\mathbf{q}_w = \phi(\mathbf{v}_f - \mathbf{v}_s)$, $\mathbf{v}_s = \partial_t \mathbf{u}$ denotes the soil skeleton velocity, deduced from the displacement of soil skeleton \mathbf{u} .

2.2. Darcy's law

In this study, the flow in the porous medium is governed by Darcy's law:

$$\mathbf{q}_w = -\frac{k(\phi)}{\eta_k \bar{\rho}(c)} (\text{grad}(p_w) - \bar{\rho}(c) \mathbf{g}) \quad (9)$$

where k is the intrinsic permeability of the medium depended on porosity (Yang et al. 2017), η_k is the kinematic viscosity of the fluid, p_w is the pore fluid pressure, \mathbf{g} is the gravity vector, $\bar{\rho}$, ρ_s and ρ_f are the density of the mixture, the solid and the fluid:

$$\bar{\rho} = c\rho_s + (1-c)\rho_f \quad (10)$$

$$k = k_0 \frac{\phi^{k_1}}{(1-\phi)^{k_2}} \quad (11)$$

2.3. Constitutive equation for mass exchange

Eqs. (5)-(8) do not suffice for solving a boundary value problem, as the mass exchange term needs also to be formulated. A model for the rate of the eroded mass, suggesting that erosion is mainly driven by the discharge of the fluidized particles $c|q_w|$, is given by the following relation (Vardoulakis et al. 1996):

$$\hat{n} = \beta c |q_w| \quad (12)$$

where β is a material parameter determined experimentally.

2.4. Balance of linear momentum

The model has been developed for geotechnical applications and it is not the aim of the present study to present the thermodynamical setting of the erosion model. Therefore, the linear momentum balance equation of a constituent is given as follows under isothermal and quasi-static conditions:

$$\text{div}(\boldsymbol{\sigma}_i) + \rho_i \mathbf{w} + \hat{\mathbf{p}}_i = 0, \quad \sum_i \hat{\mathbf{p}}_i = 0 \quad (13)$$

where $\boldsymbol{\sigma}_i$ is the total Cauchy stress tensor of the solid or liquid phase; \mathbf{w} is the body force vector, $\hat{\mathbf{p}}_i$ is the interaction force between solid and liquid phases. In this configuration, further density driven momentum production (see Steeb and Diebels 2003) and body forces are not taken into account. Nevertheless, we assume that the process is slow, i.e. the inertia forces can be neglected. This equilibrium equation allows prescribing the total force $\mathbf{t} = \boldsymbol{\sigma} \cdot \mathbf{n}$ and the solid displacement \mathbf{u}_s at the boundary of the body. Thus the set of equations (5)-(8) can be closed by:

$$\sigma'_{ij,i} + p_{w,i} = w_i \quad (14)$$

where σ'_{ij} denotes the component of the effective stress tensor, p_w the pore pressure, w the averaged body force per unit volume.

3. NUMERICAL ITEGRATION

Together with Eqs. (5)-(8), (12) and (14), a system of 5 equations for 5 unknowns ($\mathbf{u}, p_w, \phi, c, \mathbf{q}_w$) was obtained: the soil skeleton displacement (\mathbf{u}), the pore pressure (p_w), the porosity (ϕ), the concentration of fluidized particle (c) and the total discharge of liquid (\mathbf{q}_w). This coupled mechanical-erosion process is a non-linear transient problem. Weak forms of the governing equation system were implemented in a finite element code ABAQUS (Hibbitt et al. 2001). The weak forms were linearized and solved iteratively at each time step with the Newton-Raphson method. The non-linear system can be written in a compact form:

$$\mathbf{R}(u, p_w, \phi, c, q_w) = 0 \quad (15)$$

where \mathbf{R} is the vector of residuals. Giving an initial approximation $y^{(0)}$ to the solution y , the $(m+1)$ th approximation was obtained from the m th by solving:

$$\mathbf{J}_{(m)} [\mathbf{y}_{(m+1)} - \mathbf{y}_{(m)}] = -\mathbf{R}_{(m)} \quad (16)$$

where \mathbf{J} is the Jacobian matrix which contains the partial derivatives of the residuals \mathbf{R} with respect to the

unknowns, i.e. $J_{ij} = (\partial R^i / \partial x_j)$. The integer m is the iteration counter. The linearized forms of the weak forms are then derived as:

$$\begin{pmatrix} \frac{\partial R_1}{\partial u} & \frac{\partial R_1}{\partial p_w} & 0 & 0 & 0 \\ \frac{\partial R_2}{\partial u} & \frac{\partial R_2}{\partial p_w} & \frac{\partial R_2}{\partial \phi} & \frac{\partial R_2}{\partial c} & 0 \\ \frac{\partial R_3}{\partial u} & 0 & \frac{\partial R_3}{\partial \phi} & \frac{\partial R_3}{\partial c} & \frac{\partial R_3}{\partial q_w} \\ \frac{\partial R_4}{\partial u} & 0 & \frac{\partial R_4}{\partial \phi} & \frac{\partial R_4}{\partial c} & \frac{\partial R_4}{\partial q_w} \\ 0 & \frac{\partial R_5}{\partial p_w} & \frac{\partial R_5}{\partial \phi} & \frac{\partial R_5}{\partial c} & \frac{\partial R_5}{\partial q_w} \end{pmatrix}_{(m)} \begin{pmatrix} \delta u \\ \delta p_w \\ \delta \phi \\ \delta c \\ \delta q_w \end{pmatrix}_{(m+1)} = - \begin{pmatrix} R_1 \\ R_2 \\ R_3 \\ R_4 \\ R_5 \end{pmatrix}_{(m)} \quad (17)$$

In the finite element formulation, the Galerkin method was used. An isoparametric 8-node element was developed and implemented into the finite element code ABAQUS. The soil skeleton displacement (\mathbf{u}) was approximated at 8 nodes, whereas the other 4 unknowns ($p_w, \phi, c, \mathbf{q}_w$) were approximated at 4 nodes to ensure the Inf-Sup or LBB condition (Babuška 1973; Brezzi 1974; Ladyzhenskaya 1969).

4. VERIFICATION

The proposed numerical approach was firstly applied to simulate the wellbore erosion problem defined by Stavropoulou et al. (1998). An erosion law which considers plugging as a higher-order effect was used:

$$\hat{n} = \beta(1 - \phi) \left(c - \frac{c^2}{c_{cr}} \right) |\mathbf{q}_w| \quad (18)$$

where c_{cr} denotes the critical value of c for which the two competing phenomena, erosion and plugging, balance each other. The obtained results were then compared to the published results of Stavropoulou in order to validate the proposed numerical approach.

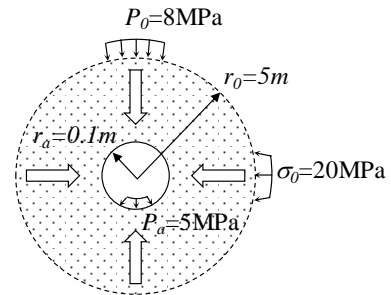


Fig. 2 Geometric and boundary conditions for the wellbore erosion problem

Fig. 2 illustrates the horizontal section of a wellbore in deep rock (Stavropoulou et al. 1998), which is treated as a porous and permeable material. A water pressure gradient initialized a fluid flow towards the inner free

surface of the wellbore, a process leading to internal erosion. The mechanical behaviour of the soil skeleton was assumed to be elastic. The initial porosity was $\phi_0 = 0.25$, the initial concentration of fluidized particles $c_0 = 0.001$, the erosion coefficient $\beta = 5m^{-1}$. More details can be found in Stavropoulou et al. (1998).

In this example, the material was assumed to be non-linear elastic, whereas the rock elasticity is assumed to depend on the porosity in such a way that the material becomes weaker with the increase of porosity:

$$E = \bar{E}(1 - \phi) \quad (19)$$

where \bar{E} is the Young's modulus, and the porosity ϕ is a damage parameter.

Fig. 3 shows the spatial profiles of porosity and pore pressure at various time steps. Fig. 4 shows the distribution of tangential effective stress at various time steps. The results of the 2D plane strain simulation are in good agreement with the results of the axisymmetric analysis carried out by Stavropoulou et al. (1998). The slight differences might be related to the time increment and the mesh size, which were not given in Stavropoulou et al. (1998).

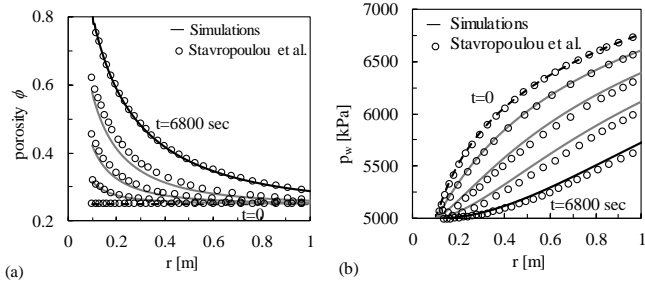


Fig. 3 Spatial profiles of porosity and pore pressure at various time steps

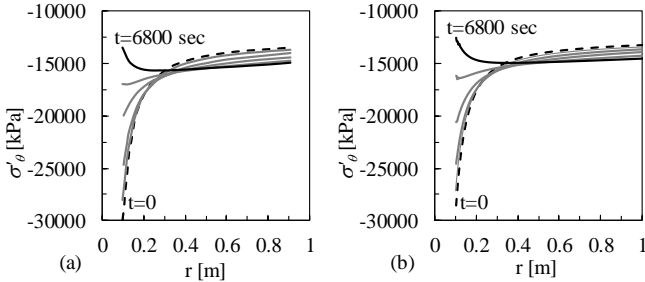


Fig. 4 Distribution of tangential effective stress at various time steps: (a) Results of Stavropoulou et al. 1998; (b) Simulation results

5. NUMERICAL MODELING OF INTERNAL EROSION WITHIN A DIKE

5.1. Description of the problem

The characteristics of the studied configuration are presented in Fig. 5 according to the typical cross section

of the dike of Val d'Orléans (Alboresha 2016). The dike was built on sandy-silt alluvium formation over karstic limestones. A confined aquifer under pressure is located underneath the limestone layer. It can rise inside the karstic caves and even reach the alluvium layer. Internal erosion due to seepage flow can take place when the water level is different in the alluvium and in the confined aquifer. The computations aim to show how the internal erosion may weaken the foundation and the dike, which will eventually lead to subsidence or collapse of the dike. The problem is analyzed under the assumption of a plane strain condition. The water level is located at the top of the dike, *i.e.*, 10.5 m, as the extreme configuration of a flooding condition is considered. The dike is assumed to be initially stable under gravity and the water head of the confined aquifer is assumed to be 11.0m. Presumably, a karst collapse underneath the alluvium layer leads to a cavity connecting the alluvium and the confined aquifer where erosion can occur due to the existence of local hydraulic gradients in the vicinity of the cavity. To simplify, the influence of the size of the cavity was not considered, the cavity was assumed to be localized at a single point of the model.

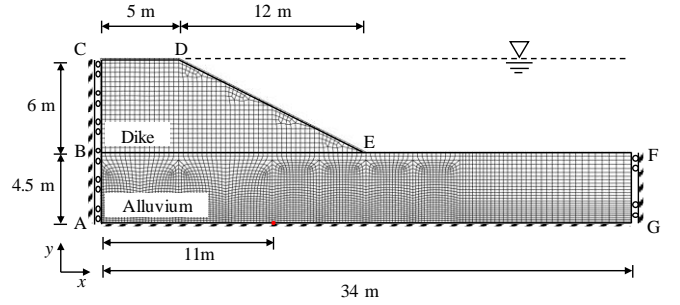


Fig. 5 Scheme of the specific dike example

5.2. A sand-silt mixture model for the solid phase

The alluvium and the dike were considered to be made of the same mixture of sand and silt. A non-associated elastoplastic model for sand-silt mixture (Yin et al. 2016) has been adopted. This model has been extended from the basic SIMSAND model (Jin et al. 2016a; Jin et al. 2016b; Wu et al. 2017) under the framework of the critical state concept and elastoplasticity theory (summarized in Table 1), by the incorporation of the position of the critical state line as a function of the fines content in order to unify the mechanical behavior of a sand-silt mixture from silt to sand or sand to silt. A non-linear expression of the critical state line was adopted as follows:

$$e_c = e_{cr0} - \lambda(p'/p_{at})^\xi \quad (20)$$

where e_{cr0} is the reference critical void ratio corresponding to the void ratio e at the mean effective stress $p' = 0$. It determines the position of the CSL in the $e - p'$ plane. λ and ξ are material constants controlling the non-linear expression of the CSL. According to Yin et

al. 2016, e_{cr0} is considered as a function of the fines content in order to unify the mechanical behavior of a sand-silt mixture for different fines contents:

$$e_{cr0} = \left[e_{hc,cr0} (1 - f_c) + a f_c \right] \frac{1 - \tanh[\zeta (f_c - f_{th})]}{2} + e_{hf,cr0} \left(f_c + \frac{1 - f_c}{(R_d)^m} \right) \frac{1 + \tanh[\zeta (f_c - f_{th})]}{2} \quad (21)$$

where $e_{hc,cr0}$ and $e_{hf,cr0}$ are the reference critical void ratios for the pure sand and pure silt, respectively; a controls the slope of the curve for the silty sand; m controls the slope of the curve for the sandy silt; f_{th} and ζ control the transition zone between the silty sand and the sandy silt. R_d is the ratio of the mean size of the coarse grains D_{50} to the mean size of the fine grains d_{50} . Therefore, this model is able to take into account the influence of the change of porosity and the fines content on the mechanical behavior of the soil during the erosion process.

Table 1 Basic constitutive equations of SIMSAND

Components	Constitutive equations
Elasticity	$\dot{\epsilon}_{ij}^e = \frac{1 + \nu}{3K(1 - 2\nu)} \sigma'_{ij} - \frac{\nu}{3K(1 - 2\nu)} \sigma'_{kk} \delta_{ij}$ $K = K_0 \cdot p_{at} \frac{(2.97 - e)^2}{1 + e} \left(\frac{p'}{p_{at}} \right)^\xi$
Yield surface in shear	$f_s = q/p' - H$
Potential surface in shear	$\frac{\partial g_s}{\partial p'} = A_d \left(M_{pt} - \frac{q}{p'} \right); \quad \frac{\partial g_s}{\partial s_{ij}} = \{1 \ 1 \ 1 \ 1 \ 1\}$
Hardening rule for shear	$H = M_p \varepsilon_d^p / (k_p + \varepsilon_d^p)$
Critical state line and interlocking effect	$\tan \phi_p = (e_c/e) \tan \phi_\mu; \tan \phi_{pt} = (e/e_c) \tan \phi_\mu$ $e_c = e_{cr0} - \lambda (p'/p_{at})^\xi$

* K is the bulk modulus; ν is the Poisson's ratio; p_{at} is the atmospheric pressure ($p_{at} = 101.325$ kPa); p' is the mean effective stress; q is the deviatoric stress; k_p is the plastic shear modulus; A_d is the stress-dilatancy parameter; ϕ_p is peak friction angle; ϕ_{pt} is phase transformation friction angle; ϕ_μ is critical friction angle; M_p and M_{pt} is the stress ratio corresponding to peak strength and phase transformation strength respectively; e_c is the critical void ratio; e_{cr0} is the reference critical void ratio corresponding to $p_{ref} = p_{at}$; λ is the slope of the CSL in the e - $\log p'$ plane.

The physical properties and the material parameters correspond to the Ottawa 50/200 sand-silt characteristics (Yin et al. 2016) with $e_0 = 0.6$, $c_0 = 0.01$ and $f_{c0} = 0.4$ have been adopted in this analysis. A residual fines content was artificially given for the sake of simplicity ($f_{c,r} = 0.3$).

5.3. Hydro-mechanical responses induced by internal erosion

Fig. 6 shows the evolution with time of the void ratio inside the dike and the underlying soil foundation. As internal erosion takes place, the void ratio, which is initially spatially uniform throughout the whole model, begins to increase with time. The void ratio increase starts at the vicinity of the cavity where a highly eroded zone appears and develops towards the dike, following the direction of the maximum hydraulic gradient. At places where the fines content reaches the residual fines content, it is assumed that the erosion process is balanced by the filtration process and, as a consequence, the void ratio will no longer change, but the size of the eroded area will continue to develop.

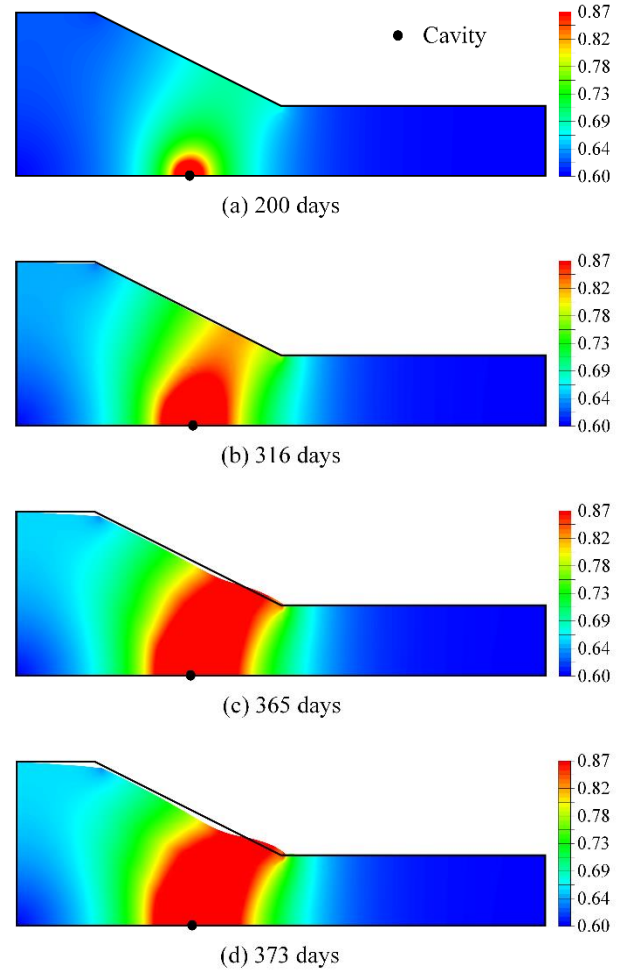


Fig. 6 Spatial distribution of void ratio at different times

Fig. 7 show the deviatoric plastic strain fields within the deformed dike at the corresponding times of Fig. 6. The displacements were reset after the initiation of the stresses by gravity. The increase of the void ratio accompanied by a downward shift of the CSL in the e - p' plane induced by the decrease of the fines content makes the soil looser. As a consequence, the soil resistance decreases. Two stages can be distinguished from the results. Plastic deformation initiates in the vicinity of the cavity. The deformation of the dike develops at a fairly slow pace at the early stage

of the erosion when the eroded zone is concentrated in the foundation. At this stage, the soil moves downwards to the cavity, as the eroded zone around the cavity is weaker.

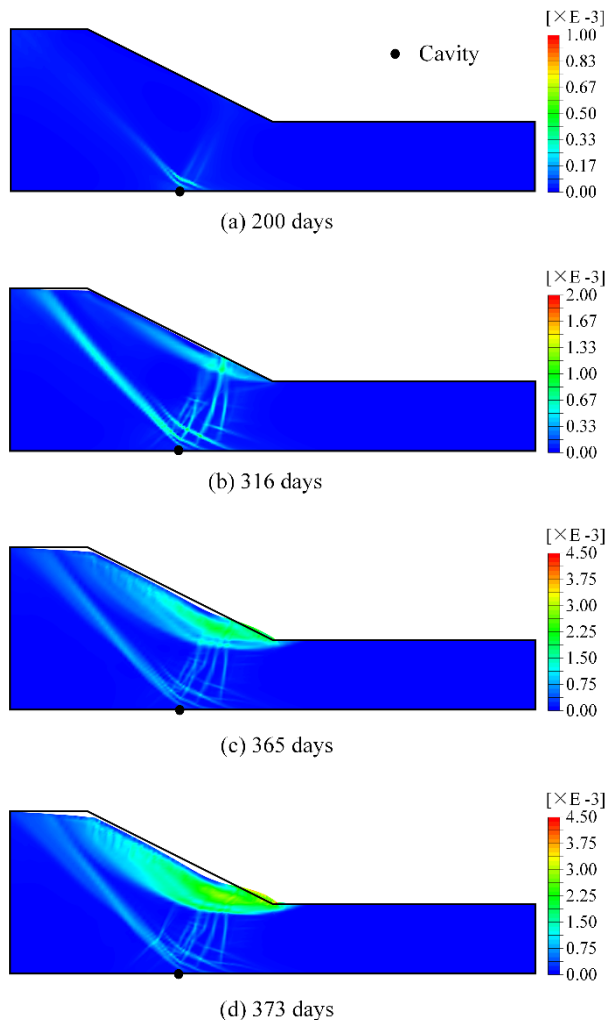


Fig. 7 Deviatoric plastic strain field at different times

The rate of the deformation keeps increasing with the development of the eroded zone, confirmed by the time variation of the displacement magnitude, as shown in Fig. 8. 316 days after the beginning of erosion, a measurable deformation of the dike appears, accompanied by the initiation of a shear sliding surface in the eroded zone near the toe of the slope. At this stage, the plastic deformation develops drastically with time until the dike is destroyed by a sliding rupture of the slope. It should be noted that this simulation is an example under extreme conditions, where the soil cohesion has not been considered, and the dike is immersed. The decrease of the fines content, in this case, leads to the decrease of e_{cr0} . Furthermore, the hydro-mechanical responses also depend on the location of the cavity, the rate of erosion, the initial and the residual fines content, which will be discussed in the future.

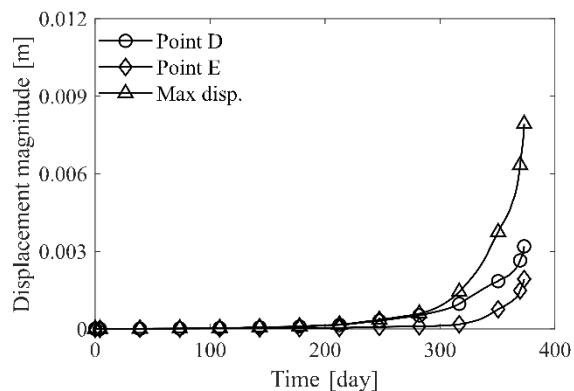


Fig. 8 Time variation of displacement magnitude at point D, point E, and maximum displacement

6. CONCLUSION

This study attempted to provide a novel contribution to the numerical approach for modelling the internal erosion of soils. The work consisted of modelling the internal erosion of the soil skeleton and the transport of fine particles by the fluid through the mass exchange between the solid skeleton and the pore water. The governing differential equations were formulated based on the balance of four assumed constituents, and then implemented into a finite element code. The code was validated via the comparison with a wellbore erosion simulation (Stavropoulou et al. 1998). In addition, an elasto-plastic sand-silt mixture constitutive model considering the fines content effect was used to take into account the hydro-mechanical coupling induced by internal erosion.

The example of a dike demonstrated the applicability of the model to simulate the evolution of internal erosion with time on a real scale problem. The effects of internal erosion led to an increase of the index void ratio of the soil and a loss of fines content, which in turn resulted in the decrease of the shear strength of the eroded zone, evaluated by a sand-silt mixture constitutive model. In this case, the numerical results showed that the deformation of the dike developed rather slowly when the eroded zone was concentrated within the foundation. A measurable deformation within the dike appeared when the eroded zone developed towards the slope area. It increased dramatically until the dike failed suddenly due to a sliding rupture of the slope.

ACKNOWLEDGEMENT

The financial supports provided by the National Natural Science Foundation of China (51579179) and the National Institute for Industrial Environment and Risks of France (INERIS) are gratefully acknowledged. The support provided by the GDRI GeoMech is gratefully acknowledged.

REFERENCES

1. Alboresha, R. 2016. Evaluation of the impact of a cavity upon an earth dike (analytical and numerical approaches): Application to the Val d'Orléans area (France). Université de Lorraine.
2. Babuška, I. 1973. The finite element method with Lagrangian multipliers. *Numerische Mathematik*, **20**(3): 179-192.
3. Bear, J., and Bachmat, Y. 2012. Introduction to modeling of transport phenomena in porous media. Springer Science & Business Media.
4. Bendahmane, F., Marot, D., and Alexis, A. 2008. Experimental parametric study of suffusion and backward erosion. *Journal of geotechnical and geoenvironmental engineering*, **134**(1): 57-67.
5. Bendahmane, F., Marot, D., Rosquoët, F., and Alexis, A. 2006. Characterization of internal erosion in sand kaolin soils: Experimental study. *Revue européenne de génie civil*, **10**(4): 505-520.
6. Brezzi, F. 1974. On the existence, uniqueness and approximation of saddle-point problems arising from Lagrangian multipliers. *Revue française d'automatique, informatique, recherche opérationnelle. Analyse numérique*, **8**(R2): 129-151.
7. Chang, D., and Zhang, L. 2011. A stress-controlled erosion apparatus for studying internal erosion in soils. *Geotechnical Testing Journal*, **34**(6): 579-589.
8. Cividini, A., and Gioda, G. 2004. Finite-element approach to the erosion and transport of fine particles in granular soils. *International Journal of Geomechanics*, **4**(3): 191-198.
9. de Boer, R. 2000. Contemporary progress in porous media theory. *Applied Mechanics Reviews*, **53**(12): 323-370.
10. Fujisawa, K., Murakami, A., and Nishimura, S.-i. 2010. Numerical analysis of the erosion and the transport of fine particles within soils leading to the piping phenomenon. *Soils and foundations*, **50**(4): 471-482.
11. Hibbitt, Karlsson, and Sorensen. 2001. ABAQUS/standard User's Manual. Hibbitt, Karlsson & Sorensen.
12. Jin, Y.-F., Yin, Z.-Y., Shen, S.-L., and Hicher, P.-Y. 2016a. Investigation into MOGA for identifying parameters of a critical-state-based sand model and parameters correlation by factor analysis. *Acta Geotechnica*, **11**(5): 1131-1145.
13. Jin, Y.F., Yin, Z.Y., Shen, S.L., and Hicher, P.Y. 2016b. Selection of sand models and identification of parameters using an enhanced genetic algorithm. *International journal for numerical and analytical methods in geomechanics*, **40**(8): 1219-1240.
14. Ladyzhenskaya, O.A. 1969. The mathematical theory of viscous incompressible flow. No. 3. Gordon & Breach New York.
15. Lominé, F., Scholtès, L., Sibille, L., and Poullain, P. 2013. Modeling of fluid–solid interaction in granular media with coupled lattice Boltzmann/discrete element methods: application to piping erosion. *International journal for numerical and analytical methods in geomechanics*, **37**(6): 577-596.
16. Marot, D., Rochim, A., Nguyen, H.-H., Bendahmane, F., and Sibille, L. 2016. Assessing the susceptibility of gap-graded soils to internal erosion: proposition of a new experimental methodology. *Natural Hazards*, **83**(1): 365-388.
17. Moffat, R., Fannin, R.J., and Garner, S.J. 2011. Spatial and temporal progression of internal erosion in cohesionless soil. *Canadian Geotechnical Journal*, **48**(3): 399-412.
18. Reboul, N. 2008. Transport de particules dans les milieux granulaires: Application à l'érosion interne. Ecully, Ecole centrale de Lyon.
19. Reddi, L.N., Lee, I.-M., and Bonala, M.V. 2000. Comparison of internal and surface erosion using flow pump tests on a sand-kaolinite mixture. *Geotechnical Testing Journal*, **23**(1): 116-122.
20. Sari, H., Chareyre, B., Catalano, E., Philippe, P., and Vincens, E. Investigation of internal erosion processes using a coupled dem-fluid method. *In Particles 2011 II International Conference on Particle-Based Methods*, E. Oate and DRJ Owen (Eds), Barcelona. 2011. pp. 1-11.
21. Schaufler, A., Becker, C., and Steeb, H. 2013. Infiltration processes in cohesionless soils. *ZAMM - Journal of Applied Mathematics and Mechanics/Zeitschrift für Angewandte Mathematik und Mechanik*, **93**(2 - 3): 138-146.
22. Scholtès, L., Hicher, P.-Y., and Sibille, L. 2010. Multiscale approaches to describe mechanical responses induced by particle removal in granular materials. *Comptes Rendus Mécanique*, **338**(10-11): 627-638.
23. Sibille, L., Lominé, F., Poullain, P., Sail, Y., and Marot, D. 2015. Internal erosion in granular media: direct numerical simulations and energy interpretation. *Hydrological Processes*, **29**(9): 2149-2163.
24. Skempton, A., and Brogan, J. 1994. Experiments on piping in sandy gravels. *Géotechnique*, **44**(3): 449-460.
25. Stavropoulou, M., Papanastasiou, P., and Vardoulakis, I. 1998. Coupled wellbore erosion and stability analysis. *International journal for numerical and analytical methods in geomechanics*, **22**(9): 749-769.
26. Sterpi, D. 2003. Effects of the erosion and transport of fine particles due to seepage flow. *International Journal of Geomechanics*, **3**(1): 111-122.
27. Vardoulakis, I., Stavropoulou, M., and Papanastasiou, P. 1996. Hydro-mechanical aspects of the sand production problem. *Transport in porous media*, **22**(2): 225-244.
28. Wong, H., Zhang, X., Leo, C., and Bui, T. 2013. Internal Erosion of earth structures as a coupled hydromechanical process. *In Applied Mechanics and Materials*. Trans Tech Publ. pp. 1084-1089.
29. Wu, Z.-X., Yin, Z.-Y., Jin, Y.-F., and Geng, X.-Y. 2017. A straightforward procedure of parameters determination for sand: a bridge from critical state based constitutive modelling to finite element analysis. *European Journal of Environmental and Civil Engineering*: 1-23.
30. Yang, J., Yin, Z.-Y., Hicher, P.-Y., and Laouafa, F. 2017. A Finite Element Modeling of the Impact of Internal Erosion on the Stability of a Dike. *In Poromechanics VI*. pp. 354-361.
31. Yin, Z.-Y., Huang, H.-W., and Hicher, P.-Y. 2016. Elastoplastic modeling of sand–silt mixtures. *Soils and foundations*, **56**(3): 520-532.
32. Zhao, J., and Shan, T. 2013. Coupled CFD–DEM simulation of fluid–particle interaction in geomechanics. *Powder technology*, **239**: 248-258.